PNAS RESEARCH ARTICLE | MEDICAL SCIENCES

MBTD1 preserves adult hematopoietic stem cell pool size and function

Keiyo Takubo[a,1], Phyo Wai Htun[b], Takeshi Ueda[c], Yasuyuki Sera[d], Masayuki Iwasaki[d], Miho Koizumi[d], Kohei Shiroshita[a], Hiroshi Kobayashi[a], Miho Haraguchi[a], Shintaro Watanuki[a], Zen-ichiro Honda[e], Norimasa Yamasaki[f], Ayako Nakamura-Ishizu[g], Fumio Arai[h], Noboru Motoyama[i], Tomohisa Hatta[j], Tohru Natsume[j], Toshio Suda[k], and Hiroaki Honda[d,1]

Edited by Hanna K. Mikkola, University of California, Los Angeles, CA; received April 20, 2022; accepted June 28, 2023 by Editorial Board Member Brigid L. Hogan

Mbtd1 (mbt domain containing 1) **encodes a nuclear protein containing a zinc finger domain and four malignant brain tumor (MBT) repeats. We previously generated *Mbtd1*-deficient mice and found that MBTD1 is highly expressed in fetal hematopoietic stem cells (HSCs) and sustains the number and function of fetal HSCs. However, since *Mbtd1*-deficient mice die soon after birth possibly due to skeletal abnormalities, its role in adult hematopoiesis remains unclear. To address this issue, we generated *Mbtd1* conditional knockout mice and analyzed adult hematopoietic tissues deficient in *Mbtd1*. We observed that the numbers of HSCs and progenitors increased and *Mbtd1*-deficient HSCs exhibited hyperactive cell cycle, resulting in a defective response to exogenous stresses. Mechanistically, we found that MBTD1 directly binds to the promoter region of *FoxO3a*, encoding a forkhead protein essential for HSC quiescence, and interacts with components of TIP60 chromatin remodeling complex and other proteins involved in HSC and other stem cell functions. Restoration of FOXO3a activity in *Mbtd1*-deficient HSCs in vivo rescued cell cycle and pool size abnormalities. These findings indicate that MBTD1 is a critical regulator for HSC pool size and function, mainly through the maintenance of cell cycle quiescence by FOXO3a.**

MBTD1 (mbt domain containing 1) | hematopoietic stem cells (HSCs) | HSC quiescence | FOXO3a

Significance

MBTD1 is an intranuclear protein whose function is poorly understood. By generating *Mbtd1* conditional knockout mice, we demonstrated that MBTD1 is an essential regulator in adult hematopoiesis. In adult hematopoietic stem cells (HSCs), we found that MBTD1 directly binds to the promoter region of *FoxO3a*, encoding a key regulator of HSC quiescence and interacts with ribosomal as well as other proteins essential for HSC function. The results revealed that MBTD1 maintains adult HSC pool size and function, partly through FOXO3a-dependent cell cycle quiescence. Our findings demonstrate the essential contribution of a putative epigenetic modulator to the regulatory mechanisms of HSCs.

Lifetime hematopoiesis in mammals is sustained by the activities of hematopoietic stem/progenitor cells (HSPCs). During steady-state hematopoiesis, the majority of hematopoietic stem cells (HSCs) remain in a quiescent (G0) state or quiescence in the cell cycle in the bone marrow (BM) (1–3). Upon hematological stresses including chemotherapeutic agents, transplantation, or infection, quiescent HSCs activate their metabolism, enter the cell cycle for proliferation, and differentiate into multipotent progenitors (MPPs), which actively proliferate and differentiate into lineage-committed progenitors to support the regeneration of the hematopoietic system (4, 5). One of the key mechanisms maintaining HSC integrity is cell cycle regulation, and recent studies revealed that the cell cycle regulation of HSPCs is coordinated by metabolic machinery (6). In a previous study, we demonstrated that transplantation or cytokine stimulation activates p38MAPK and its downstream signaling in HSCs to activate purine metabolism and provide the nucleic acid pool required for HSC proliferation (7). However, the mechanisms underlying the coordinate cell cycle and metabolic activation regulating HSCs remain incompletely understood.

Mbtd1 (*mbt domain containing 1,* also denoted as *hemp, hematopoietic expressed mammalian polycomb*) was isolated from a highly purified HSC cDNA library of mouse fetal liver (FL) (8). It encodes a nuclear protein containing a Cys2–Cys2 zinc finger domain at the N terminus followed by four tandem malignant brain tumor (MBT) repeats (8, 9). The MBT domain was originally identified in the protein product of a *Drosophila polycomb group* (*PcG*) gene, *lethal (3) MBT* (*D-l(3)mbt*), whose recessive mutations induce the malignant transformation of larval and adult brain tissues (10). To date, a number of different MBT-containing proteins, such as L3MBTL1/H-L(3)MBT, SCMH1, and SCML2, have been identified and evolutionally classified based on the domain structures (11–13). Previous studies reported that the MBT domain recognizes lysine residues with various degrees of methylation (14, 15) and MBTD1 was recently shown to have a strong affinity to monomethylated and dimethylated histone H4 lysine 20 (H4K20) (16). In addition, subsequent studies demonstrated that MBTD1 functions as a component of TIP60 chromatin remodeling complex (17, 18). Thus, MBTD1 is considered to regulate the expression patterns of downstream genes in an epigenetic manner; however, their precise biological roles have not yet been completely elucidated.

We previously generated *Mbtd1*-deficient (*Mbtd1*$^{-/-}$) mice (9). During the early embryonic stage (E14.5), *Mbtd1*$^{-/-}$ FL contained a markedly reduced number of hematopoietic

Author contributions: K.T., P.W.H., T.U., Y.S., M.I., T.S., and H.H. designed research; K.T., P.W.H., T.U., Y.S., M.I., M.K., K.S., H.K., M.H., S.W., Z.-i.H., N.Y., A.N.-I., F.A., T.H., T.N., and H.H. performed research; N.M. contributed new reagents/analytic tools; K.T., P.W.H., T.U., Y.S., M.I., M.K., K.S., H.K., M.H., S.W., Z.-i.H., N.Y., A.N.-I., F.A., N.M., T.H., T.N., T.S., and H.H. analyzed data; and K.T. and H.H. wrote the paper.

The authors declare no competing interest.

This article is a PNAS Direct Submission. H.K.M. is a guest editor invited by the Editorial Board.

[1]To whom correspondence may be addressed. Email: keiyot@gmail.com or honda.hiroaki@twmu.ac.jp.

This article contains supporting information online at https://www.pnas.org/lookup/suppl/doi:10.1073/pnas.2206860120/-/DCSupplemental.

Published July 31, 2023.

cells. In addition, *Mbtd1*$^{-/-}$ FL HSCs possessed impaired proliferative and reconstitution abilities. Moreover, the expression levels of several genes implicated in hematopoietic development and differentiation were altered in *Mbtd1*$^{-/-}$ FL HSCs. Based on these results, we concluded that MBTD1 plays a critical role in FL HSCs, especially during the early embryonic stage, by regulating the expression patterns of FL HSC-associated genes (9). However, since *Mbtd1*$^{-/-}$ mice die soon after birth due to skeletal malformations resembling Klippel–Feil deformities (9), the role of MBTD1 in adult hematopoiesis remains unclear. In this study, we generated and analyzed *Mbtd1* conditional knockout (*Mbtd1*$^{flox/flox}$) mice and observed phenotypes supporting its requirement of adult HSCs. We demonstrated that MBTD1 regulates HSC properties by directly activating *FoxO3a* transcription and possibly through interactions with proteins including components of TIP60 chromatin remodeling complex and other proteins involved in stem cell function. Our findings reveal a crucial role of MBTD1 in adult HSC integrity by regulating HSC pool size and function.

Results

Ablation of MBTD1 in Adult Hematopoietic Tissues Induced an Increase in HSPCs and Accumulation of Myeloid Progenitors. To investigate the role of MBTD1 in adult hematopoiesis, we first examined *Mbtd1* expression patterns at various stages of hematopoietic differentiation in adult BM. RNAs extracted from cells in long-term HSC (LT-HSC), short-term HSC (ST-HSC), MPP, and lineage (Lin)$^-$, as well as Lin$^+$ fractions were subjected to quantitative real-time PCR (qRT-PCR) (surface markers of hematopoietic HSPC fractions are described in ref. 19 and summarized in *SI Appendix*, Table S1). *Mbtd1* was preferentially expressed in the LT-HSC, ST-HSC, MPP, and Lin$^-$ fractions but not in the Lin$^+$ fraction (*SI Appendix*, Fig. S1*A*). Similarly, data from a public database showed that *Mbtd1* is highly expressed in human and mouse BM HSCs compared with progenitor cells (20) (*SI Appendix*, Fig. S1*B*). These results suggest that MBTD1 may function in HSPCs in the adult BM as it does in the FL (9).

To clarify the role of MBTD1 in adult hematopoiesis, we generated *Mbtd1*$^{flox/flox}$ mice (*SI Appendix*, Fig. S2 *A* and *B*) and crossed them with interferon (IFN)-inducible *Mx1-Cre*$^+$ (*Mx1*$^+$) transgenic mice (21) to create *Mbtd1*$^{flox/flox}$/*Mx1*$^+$ mice (*Upper* two panels of *SI Appendix*, Fig. S3*A* and *Left* two lanes of *SI Appendix*, Fig. S3*B*). Administration of pIpC, a strong and transient IFN inducer, efficiently deleted the *floxed* region (*SI Appendix*, Fig. S2*C*) and almost completely abolished MBTD1 protein in the hematopoietic tissues of *Mbtd1*$^{flox/flox}$/*Mx1*$^+$ mice (*SI Appendix*, Fig. S2*D*) [hereafter, pIpC-treated *Mbtd1*$^{flox/flox}$/*Mx1*$^-$ and *Mbtd1*$^{flox/flox}$/*Mx1*$^+$ mice are referred to as *control* (*Ctrl*) and *Mbtd1 cKO* (*cKO*) mice, respectively].

The hematopoietic parameters of *Ctrl* and *cKO* mice were analyzed. At steady state, there was no significant change in the number of mononuclear cells in the thymus, spleen, and BM between *Ctrl* and *cKO* mice (*SI Appendix*, Fig. S4*A*). In addition, white blood cell (WBC) count, hemoglobin (Hb) concentration, and platelet (Plt) number in peripheral blood (PB) were comparable between the two groups (*SI Appendix*, Fig. S4*B*). Next, we investigated cell numbers of various fractions in the hematopoietic hierarchy. The cell numbers in the LSK fraction and those in the LT-HSC and ST-HSC fractions were significantly increased in the *cKO* BM compared with those in the *Ctrl* BM (Fig. 1*A*). Furthermore, accumulation of common myeloid progenitor (CMP) and granulocyte/macrophage progenitor (GMP) cells was observed in the *cKO* BM (Fig. 1*B*). We also performed CFU-C (colony-forming units in culture) and HPP-CFC (high proliferative potential colony-forming cell) assays, which assess the proliferative capacity of HSPCs, and found no apparent differences in both assays (*SI Appendix*, Fig. S4*C*). To analyze the early effect of MBTD1 deficiency on hematopoiesis, we examined HSPCs and differentiated cells of *Mbtd1*$^{flox/flox}$/*Mx1*$^-$ and *Mbtd1*$^{flox/flox}$/*Mx1*$^+$ mice at one week after pIpC administration. As shown in *SI Appendix*, Fig. S5, no changes were detected in HSPC and differentiated cell fractions, except a slight decrease in CLPs and a slight increase in MEPs. Thus, the increase in HSPCs, including LT-HSCs, ST-HSCs, CMPs, and GMPs, would be a late event which may compensate for a possible defect of *cKO* HSPCs. These results together indicate that although *Mbtd1* deficiency does not affect parameters in the hematopoietic tissues and PB, it alters the pool size of HSPCs at steady state.

Altered Regenerative Capacity of *cKO* HSCs Under Stress Conditions. One of the primary functions of HSC is to regenerate hematopoiesis following stress. We assessed the tolerance of *cKO* HSCs after hematological stresses by performing 5-fluorouracil (5-FU) treatment (22) and BM transplant (BMT) assays (23). We first analyzed the response to the 5-FU treatment, which induces apoptosis of cycling hematopoietic cells and switches HSCs from a dormant to a proliferative state. The results showed that the *cKO* PB exhibited a significant increase in WBC count and platelet number during the recovery phase (16 d after 5-FU, *Left* panel of Fig. 2*A* and *SI Appendix*, Fig. S6*A*). The proliferated WBCs were composed mostly of immature and mature granulocytes and partly of lymphocytes (*Right* panel of Fig. 2*A* and *SI Appendix*, Fig. S6*A*). We also analyzed HSPC fractions of 5-FU-treated mice after recovery (33 d after 5-FU). As shown in *SI Appendix*, Fig. S6*B*, the analysis revealed that the cell numbers of LSK, ST-HSC, and GMP fractions were significantly increased in *cKO* mice compared with *Ctrl* mice, indicating that the expansion of HSPCs in 5-FU-treated *cKO* mice still remained when PB parameters returned to normal.

Next, we performed a BMT assay, another stress-loading model for HSCs. *Ctrl* and *cKO* LT-HSCs (Ly5.2$^+$) were transplanted into lethally irradiated Ly5.1$^+$ congenic recipient mice with Ly5.1$^+$ competitor cells. The analysis of the donor-derived (Ly5.2$^+$) chimerism in the PB showed that recipients transplanted with *cKO* LT-HSCs exhibited a marked decrease in donor-derived cell percentages compared with those observed in mice transplanted with *Ctrl* LT-HSCs (*Left* panel of Fig. 2*B*). Differentiation status in the PB was almost similar between the two groups, except a decrease in T cells (*Right* panel of Fig. 2*B*), indicating an overall repopulating defect of *cKO* HSCs. The in vivo homing assays showed that the percentages of BM-homed cells in total, LSK, and Lin$^-$ fractions *per* transplanted cells in the same fractions were comparable between recipients transplanted with *Ctrl* and *cKO* BM cells (*SI Appendix*, Fig. S7), indicating that the reduced repopulating activity of *cKO* HSCs was not due to impaired homing ability but rather to other cell-intrinsic defect(s). These results together demonstrate that in adult mice, *cKO* HSCs exhibit abnormal behaviors under stressful conditions, such as hyperresponsiveness during the recovery process from 5-FU-induced BM suppression and a markedly reduced repopulation ability following BMT.

MBTD1 Maintains HSC Quiescence by Directly Binding to the Promoter Region of *FoxO3a* and Regulating the Expression of Cip/Kip Family CDK Inhibitors. To clarify the molecular mechanism(s) underlying altered functional properties of *cKO* HSCs, we searched for genes whose expression levels were affected by *Mbtd1* deficiency. RNAs extracted from LT-HSC, ST-HSC, and MPP fractions of *Ctrl* and *cKO* BMs were subjected to

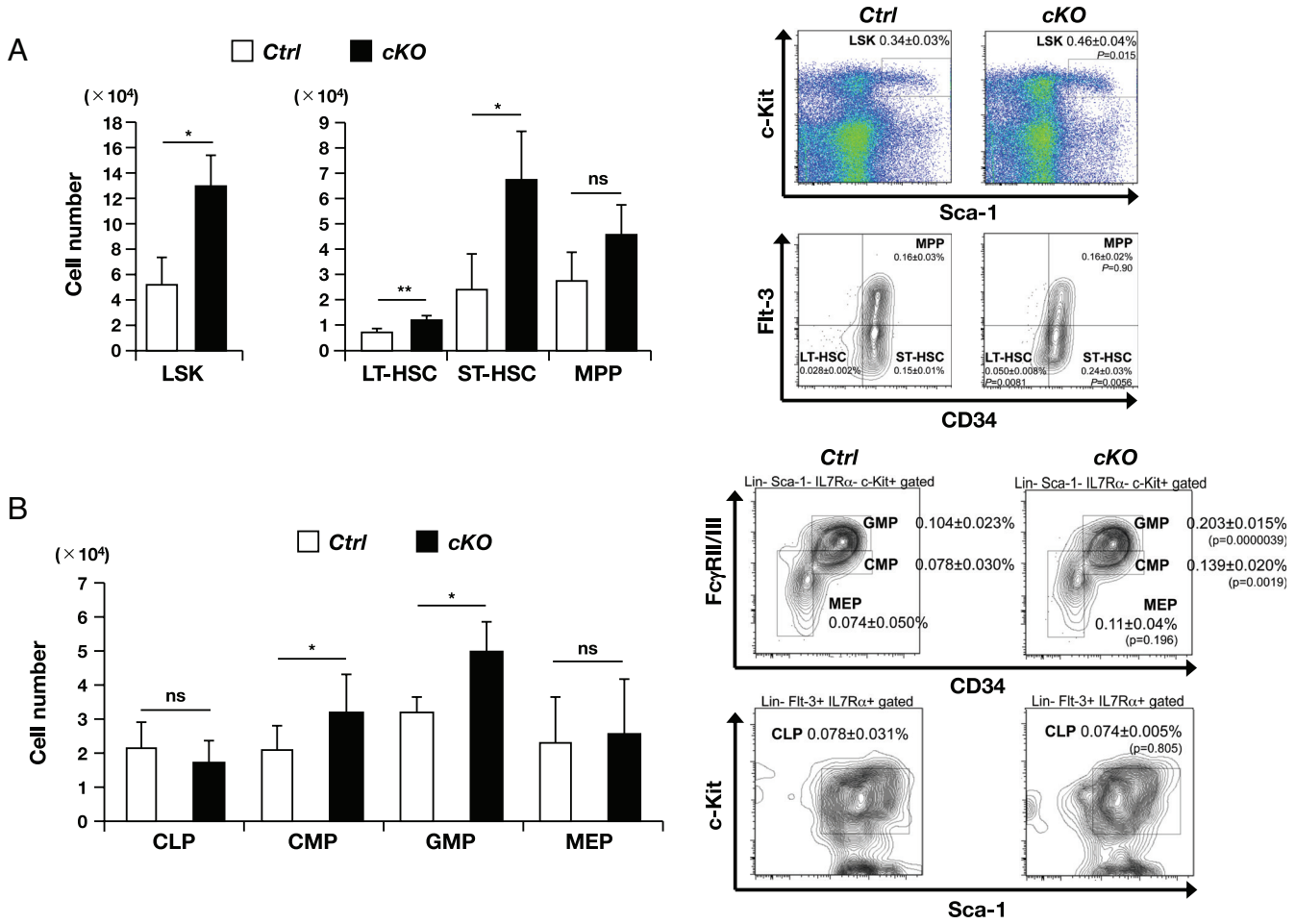

Fig. 1. Increased BM HSPC compartments in *cKO* mice. (*A*) Cell numbers (bar graphs) and frequencies (flow cytometric plots) of LSK cells, LT-HSCs, ST-HSCs, and MPPs in the BM of *Ctrl* and *cKO* mice. Cell numbers (mean ± SD, n = 5) and representative plots are shown. $^{**}P < 0.01$, $^{*}P < 0.05$, ns: not significant. (*B*) Cell numbers (bar graphs) or frequencies (flow cytometric plots) of CLPs, CMPs, GMPs, and MEPs in the BM of *Ctrl* and *cKO* mice (mean ± SD, n = 5). Cell numbers (mean ± SD, n = 5) and representative plots are shown. $^{*}P < 0.05$, ns: not significant.

qRT-PCR array analysis (Fluidigm) (24) (genes used for Fluidigm are summarized in *SI Appendix*, Table S2). Since the phenotypes observed in *cKO* mice were thought to be induced by abnormalities at the LT-HSC level, we focused on the LT-HSC fraction. We found that the expression levels of three genes, *FoxO3a*, *Egr4*, and *Tcf3*, were significantly reduced in *cKO* LT-HSC fraction compared with *Ctrl* LT-HSC fraction (*SI Appendix*, Fig. S8*A*), and qRT-PCR confirmed significant downregulation of these genes in *cKO* LT-HSCs compared with *Ctrl* LT-HSCs (*Left* panel in Fig. 3*A* and *SI Appendix*, Fig. S8*B*). We focused on *FoxO3a*, since previous studies, including ours, have demonstrated that FoxO transcriptional factors play a pivotal role in HSC function through the maintenance of cell cycle quiescence (25, 26), and the behaviors of *cKO* mice under stressful conditions, such as 5-FU stimulation and BMT (Fig. 2 *A* and *B*), closely resembled those reported in *FoxO3a* KO mice (22, 26).

To confirm the contribution of FOXO3a to the phenotypes of *cKO* mice, we examined the expression of FOXO3a protein in HSCs of *Ctrl* and *cKO* mice. As shown in the *Middle* panel of Fig. 3*A*, intracellular FACS demonstrated that the expression of FOXO3a protein was significantly reduced in *cKO* LT-HSCs compared with *Ctrl* LT-HSCs. Previous studies showed that nuclear localization of FOXO3a is essential for HSC quiescence (26, 27). Thus, we examined subcellular localization of FOXO3a by intracellular staining and measured the percentages of cytoplasmic and nuclear staining patterns in LT-HSC and ST-HSC fractions. As shown in the *Right* panel of Fig. 3*A*, the percentage of LT-HSCs localizing FOXO3a to the nucleus was reduced in *cKO* LT-HSCs compared with *Ctrl* LT-HSCs, whereas the percentage of the two staining patterns were almost comparable in the ST-HSC fraction. These results collectively indicate that the phenotypes of *cKO* mice were primarily due to reduction of FOXO3a expression in LT-HSCs.

FOXO3a maintains HSC quiescence by up-regulating the expression of cell cycle checkpoint genes, $p57^{Kip2}$ (*p57*), $p21^{Cip1}$ (*p21*), and $p27^{Kip1}$ (*p27*) (26), and autophagy-related genes including, *Atg4b*, *Bbc3*, *Bnip3*, *Gabarapl2*, *Prkaa2*, and *Sesn1* (28). Therefore, we quantified the expression levels of these genes between *Ctrl* and *cKO* LT-HSCs. As for cycle checkpoint genes, the expression levels of *p57* and *p21* were significantly down-regulated, whereas that of *p27* was significantly up-regulated in *cKO* LT-HSCs compared with *Ctrl* LT-HSCs (Fig. 3*B*). In contrast, none of the autophagy-related genes was down-regulated in *cKO* LT-HSCs compared with *Ctrl* LT-HSCs (*SI Appendix*, Fig. S9).

To further investigate whether the alteration in these gene expression profiles affected cell cycle status, we performed Pyronin Y staining and 5-Bromo-2′-deoxyuridine (BrdU) incorporation assay, which allow the identification of cells in the G0 resting phase and the proliferative stage, respectively (9). A significant decrease in Pyronin Y-negative cells and a significant increase in BrdU-positive cells were detected in the LT-HSC fraction of *cKO* mice, which indicates an enhanced cell cycle entry of *cKO* LT-HSCs (Fig. 3 *C* and *D*). Cell cycle analysis using Ki67 and

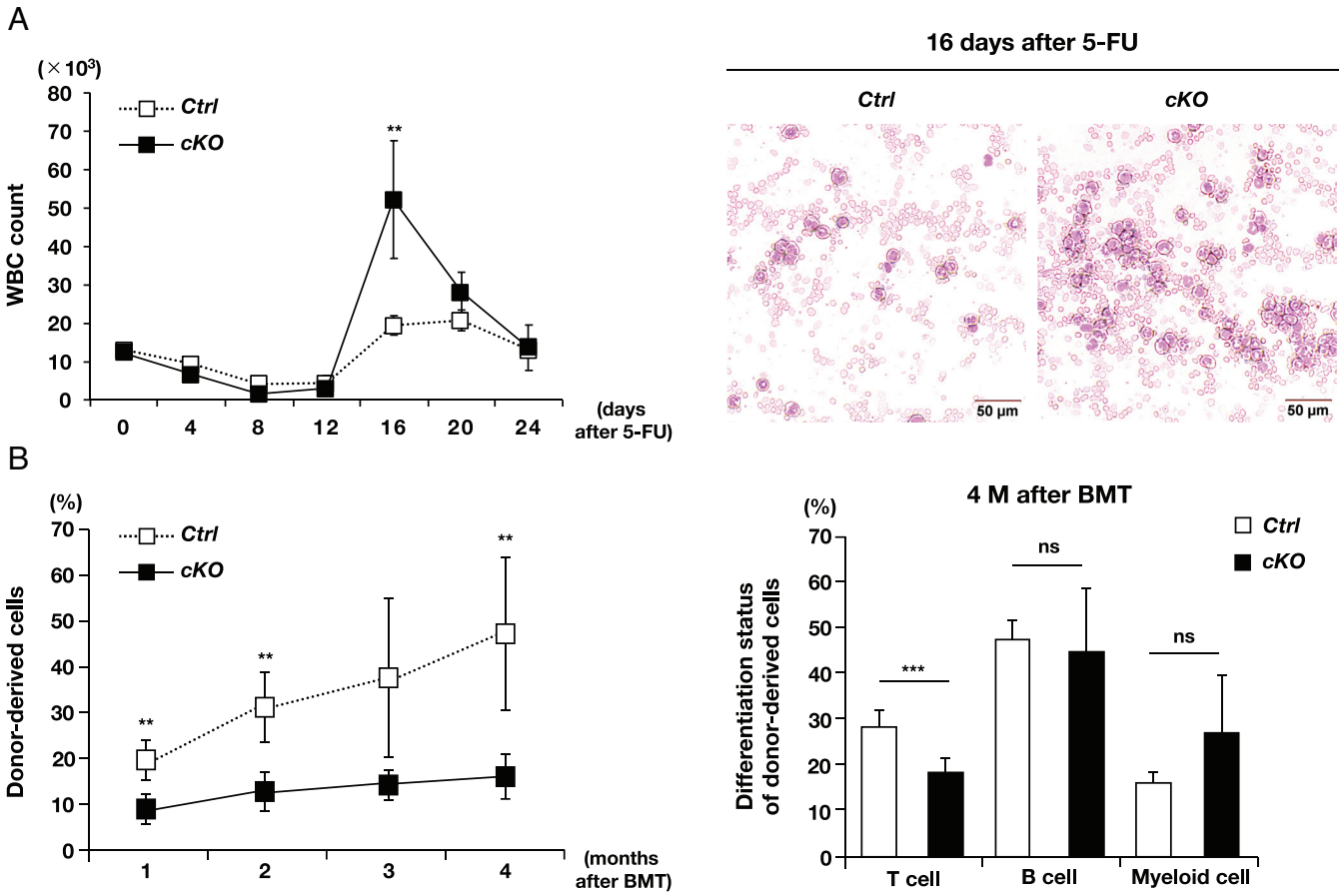

Fig. 2. Abnormal *cKO* HSC behaviors under stress conditions. (*A*) Changes in WBC count and PB images following 5-FU treatment (150 mg/kg). *Left* panel: mean WBC counts in *Ctrl* and *cKO* mice every 4 d after 5-FU injection (mean ± SD, n = 3 to 4). *Right* panel: representative PB pictures on day 16 after 5-FU injection. PB smears were stained with Wright-Giemsa. $^{**}P < 0.01$. (*B*) Chimerism and differentiation status of donor-derived cells after BM transplantation. *Left* panel: Donor-derived cells in the PB of recipient mice transplanted with *Ctrl* and *cKO* LT-HSCs at the indicated time points after BMT (mean ± SD, n = 5). *Right* panel: Percentages of T cells, B cells, and myeloid cells in the PB of *Ctrl* and *cKO* mice at 4 mo after BMT (mean ± SD, n = 5). $^{***}P < 0.001$, $^{**}P < 0.01$, ns: not significant.

Hoechst 33342 also showed that *cKO* HSCs were more active in cell cycle at steady state and after 5-FU administration (left two bars in each phase of *SI Appendix*, Fig. S10 *A* and *B*). Next, we examined the relationship between the increased stem/progenitor cell pool and the cell cycle in *cKO* HSCs. In the early phase after the pIpC administration (1 wk later) when the number of HSCs or progenitor cells did not increase (*SI Appendix*, Fig. S5), the enhanced cell cycling of *cKO* HSCs was already evident (left two bars in each phase of *SI Appendix*, Fig. S10*C*), suggesting that the first event was a change in cell cycle state of HSCs. FOXO3a deficiency enhances ERK and AKT signaling in stressed HSCs (22). Phosphorylation of ERK in HSCs was higher at steady state by *Mbtd1* deficiency, and there was no difference in the increase after 5-FU administration (*Left* panel of *SI Appendix*, Fig. S11). In contrast, phosphorylation of AKT was not different at steady state, but was significantly increased after 5-FU administration by *Mbtd1* deficiency (*Right* panel of *SI Appendix*, Fig. S11).

To investigate whether MBTD1 directly regulates *FoxO3a* transcription in HSCs, the binding ability of MBTD1 to the *FoxO3a* gene was assessed by a chromatin immunoprecipitation (ChIP) assay using LSK cells. We designed PCR primers that encompass three regions in the promoter (P1-P3) and a region in the 1st intron (P4) of the *FoxO3a* gene (*Left* panel of Fig. 3*E*). Protein-DNA complexes immunoprecipitated by control IgG or the MBTD1 antibody (9) were amplified with the primers corresponding to the P1-P4 regions. Three regions (P1, P2, and P3), located upstream of the putative transcription start site (TSS), were specifically immunoprecipitated by the MBTD1 antibody, whereas region P4, located downstream of the TSS, was not (*Right* panel of Fig. 3*E*), indicating that MBTD1 was directly recruited to the promoter region of the *FoxO3a* gene. These results demonstrate that MBTD1 contributes to HSC quiescence, at least partly, by regulating the expression of FOXO3a and downstream Cip/Kip family CDK inhibitors.

Restoration of FOXO3a Activity Recovered *cKO* HSPC Pool Size and Partially Improved Transplantation Capacity. Given the evidence of FOXO3a as a direct downstream effector of MBTD1, we designed a line of experiments for the functional assessment of the MBTD1-FOXO3a axis in hematopoiesis. To this end, we used $FoxO3a^{+/TM}$ mutant mice, in which an *floxed* Neo resistance cassette coupled with a constitutive-active mutant of *FoxO3a* cDNA ($FoxO3a^{TM}$) were knocked into the *FoxO3a* locus (26) (*SI Appendix*, Fig. S12*A*). The knockin allele functions as a *FoxO3a*-null allele at steady state; however, after Cre expression, the *floxed Neo* resistance cassette is excised and $FoxO3a^{TM}$ mRNA is expressed under the regulation of endogenous *FoxO3a* (*SI Appendix*, Fig. S12*B*). To analyze the effect of $FOXO3a^{TM}$ on normal hematopoiesis, we compared cell numbers in HSPC and differentiated cell fractions and also analyzed cell cycle of HSCs between $Mbtd1^{+/+}/Mx1^{+}/FoxO3a^{+/+}$ ($FoxO3a^{+/+}$) and $Mbtd1^{+/+}/Mx1^{+}/FoxO3a^{+/TM}$ ($FoxO3a^{+/TM}$) mice at 4 wk after pIpC treatment. As shown in *SI Appendix*, Fig. S12*C*, no changes were observed in all fractions. In addition, as shown in

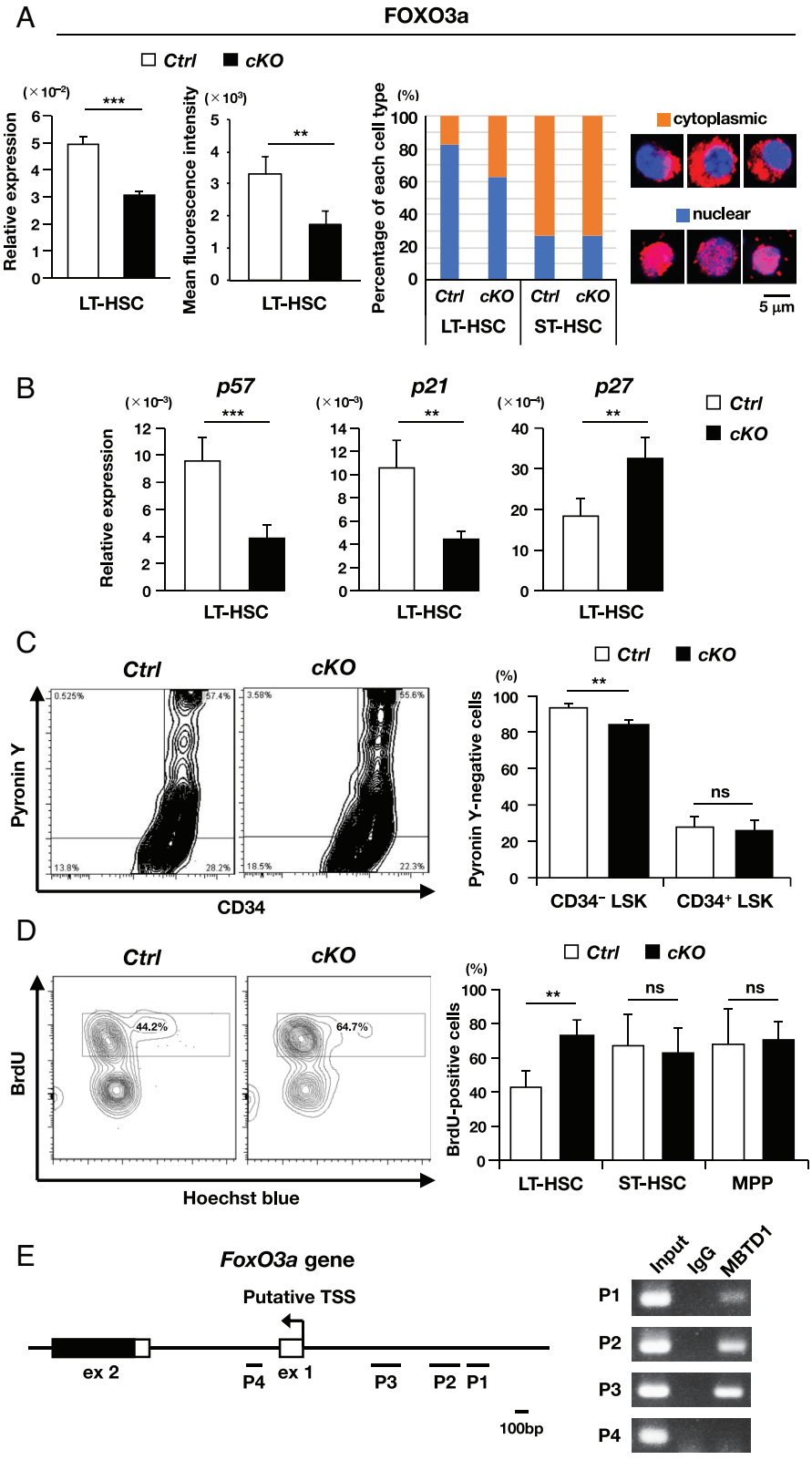

Fig. 3. Identification of MBTD1 target genes, cell cycle analyses, and MBTD1 binding to the *FoxO3a* gene. (*A*) *Left* panel: qRT-PCR of *FoxO3a* in LT-HSCs of *Ctrl* and *cKO* mice (mean ± SD, n = 4). Each value was normalized to *β-actin*. *Middle* panel: Intracellular FACS of FOXO3a in LT-HSCs of *Ctrl* and *cKO* mice (mean ± SD, n = 4). Mean fluorescence intensities are shown. *Right* panel: Intracellular staining of FOXO3a in LT-HSCs and ST-HSCs of *Ctrl* and *cKO* mice (216 to 269 cells per group). Percentages of "cytoplasmic" and "nuclear" staining patterns (representative data of two independent experiments) are shown with their representative photos. ***$P < 0.001$, **$P < 0.01$. (*B*) qRT-PCR of FOXO3a target genes, *p57p21*, and *p27*, in LT-HSCs of *Ctrl* and *cKO* mice (mean ± SD, n = 4). Each value was normalized to *β-actin*. ***$P < 0.001$, **$P < 0.01$. (*C*) Representative flow cytometric plots of Pyronin Y analysis in the LSK-gated fraction of *Ctrl* and *cKO* BM MNCs (*Left*) and the frequency of Pyronin Y-negative fraction in CD34$^-$ and CD34$^+$ LSK cells in *Ctrl* and *cKO* BM MNCs (*Right*) (mean ± SD, n = 4). **$P < 0.01$, ns: not significant. (*D*) Representative flow cytometric plots showing BrdU labeling of the LT-HSC-gated fraction from *Ctrl* and *cKO* BM mononuclear cells (MNCs, *Left*) and the frequency of the BrdU-positive fraction in LT-HSCs, ST-HSCs, and MPPs in *Ctrl* and *cKO* BM MNCs (*Right*) (mean ± SD, n = 4). **$P < 0.01$, ns: not significant. (*E*) Binding of MBTD1 to the promoter regions of the *FoxO3a* gene. *Left* panel: schematic illustration of the *FoxO3a* gene. The amplified regions used for the ChIP-PCR analysis are indicated by P1-P4, and coding and noncoding regions of the *FoxO3a* gene are shown using white and black boxes, respectively. TSS, transcription start site; ex, exon. *Right* panel: results of the ChIP-PCR analysis. The input DNA and the immunoprecipitated DNA in the control IgG (IgG) or the MBTD1 antibody (MBTD1) conditions were amplified using the PCR primers corresponding to the P1-P4 regions.

SI Appendix, Fig. S12*D*, the frequency of LT-HSCs in the G0, G1, and S/G2/M phases was comparable between *FoxO3a*$^{+/+}$ and *FoxO3a*$^{+/TM}$ groups. These results indicate that expression of FOXO3a^{TM} alone does not affect hematopoiesis, including proliferation and differentiation of HSCs.

We then crossed *Mbtd1*$^{floxl/flox}$/*Mx1*$^{+}$ mice with *FoxO3a*$^{+/TM}$ mutant mice to generate *Mbtd1*$^{floxl/flox}$/*Mx1*$^{+}$/*FoxO3a*$^{+/TM}$ mice (*SI Appendix*, Fig. S3*A* and the 3rd lane of *SI Appendix*, Fig. S3*B*). After pIpC administration, *Mbtd1*$^{floxl/flox}$/*Mx1*$^{+}$/*FoxO3a*$^{+/TM}$ mice simultaneously lost *Mbtd1* and acquired constitutively active *FoxO3a, FoxO3a*^{TM} [hereafter, pIpC-treated *Mbtd1*$^{floxl/flox}$/*Mx1*$^{+}$/*FoxO3a*$^{+/TM}$ mice are referred to as *FoxO3a*^{TM}-rescued (*Rescue*) mice]. In this model, we examined the cell numbers in HSPC fractions. We found that the increased cell numbers in the LT-HSC, ST-HSC, CMP, and GMP

fractions of *cKO* mice were successfully restored in *Rescue* mice expressing *FoxO3a*^{TM} (Fig. 4*A*). To investigate self-renewal and multilineage differentiation capacity, *Ctrl*, *cKO*, and *Rescue* LT-HSCs were transplanted into lethally irradiated recipient mice. In the 1st transplant, PB chimerism of *Rescue* LT-HSCs was significantly higher than that of *cKO* LT-HSCs (*Left* panel of Fig. 4*B*). However, in the 2nd transplant, PB chimerism of *Rescue* cells declined and was almost comparable with that of *cKO* cells, which was associated with lower chimerism in BM cell fractions of the *cKO* and *Rescue* groups than the *Ctrl* group at the end of the 2nd BMT (4 mo, *Right* panel of Fig. 4*B*). These results collectively indicate that the MBTD1-FOXO3a axis functions as a determinant of the pool size of HSPCs and partially contributes to the long-term repopulating ability of HSCs.

Restoration of FOXO3a Activity Rescued Cell Cycle Defects but Not Metabolic Alterations in *cKO* LT-HSCs. The aforementioned results demonstrated that FOXO3a^{TM} successfully rescued abnormal HSPC pool size induced by *Mbtd1* deficiency. Next, we analyzed the underlying mechanisms associated with the cell cycle quiescence and metabolic homeostasis of LT-HSCs. We first examined the cell cycle kinetics of *Ctrl*, *cKO*, and *Rescue* LT-HSCs using multicolor flow cytometry. Consistent with the *Mbtd1* deficiency-dependent increase in the LT-HSC pool (Figs. 1*A* and 4*A*), we observed a specific activation of cell cycle, characterized by a reduction in the Pyronin Y-negative G0 fraction in *cKO* CD34$^-$ LSK cells, which was recovered in *Rescue* CD34$^-$ LSK cells to the *Ctrl* level (*Left* panel of Fig. 5*A*, see also Fig. 3*C*). In contrast, the Pyronin Y-negative G0 fraction in CD34$^+$ LSK cells was comparable among the three groups (*Right* panel of Fig. 5*A*, see also Fig. 3*C*). Furthermore, short-term BrdU labeling indicated that the increase in cycling cells in the *cKO* LT-HSC fraction was returned to the *Ctrl* level by *FoxO3a*-rescue (Fig. 5*B*, see also Fig. 3*D*). Consistently, the decrease in the G0 phase fraction of *cKO* LT-HSCs in steady state and at early phase after pIpC administration was restored in the *Rescue* group (*SI Appendix*, Fig. S10 *A* and *C*). In addition, among the alteration of cell cycle regulators in *cKO* LT-HSCs (Fig. 3*B*), the decrease in *p57* and *p21* expression levels in *cKO* LT-HSCs was corrected in *Rescue* LT-HSCs, whereas, the increase in *p27* expression was further enhanced (Fig. 5*C*).

In addition to cell cycle quiescence, the metabolic property associated with ATP production is another important feature of HSCs (6). We detected significantly reduced levels of ATP in *cKO* LT-HSCs compared with those of *Ctrl* LT-HSCs, which not recovered in *Rescue* LT-HSCs (*Left* panel of Fig. 5*D*). We examined the expression levels of glycolytic genes between *Ctrl* and *cKO* LT-HSCs and found that the expression levels of *Hexikinase 2* (*Hk2*), *Enolase 2* (*Eno2*), *Enolase 3* (*Eno3*), and *Pyruvate kinase liver and red blood cell* (*Pklr*) were significantly decreased in *cKO* cells (*SI Appendix*, Fig. S13). In parallel, intracellular lactate dehydrogenase (LDH) activity, which reflects the cellular glycolytic capacity, was significantly reduced in *cKO* LT-HSCs compared with that of *Ctrl* LT-HSCs, which was not recovered in *Rescue* LT-HSCs (*Right* panel of Fig. 5*D*). These data collectively indicate that the MBTD1-FOXO3a axis specifically regulates cell cycle quiescence in LT-HSCs and suggest that MBTD1 maintains the glycolytic activity of HSCs in a FOXO3a-independent manner.

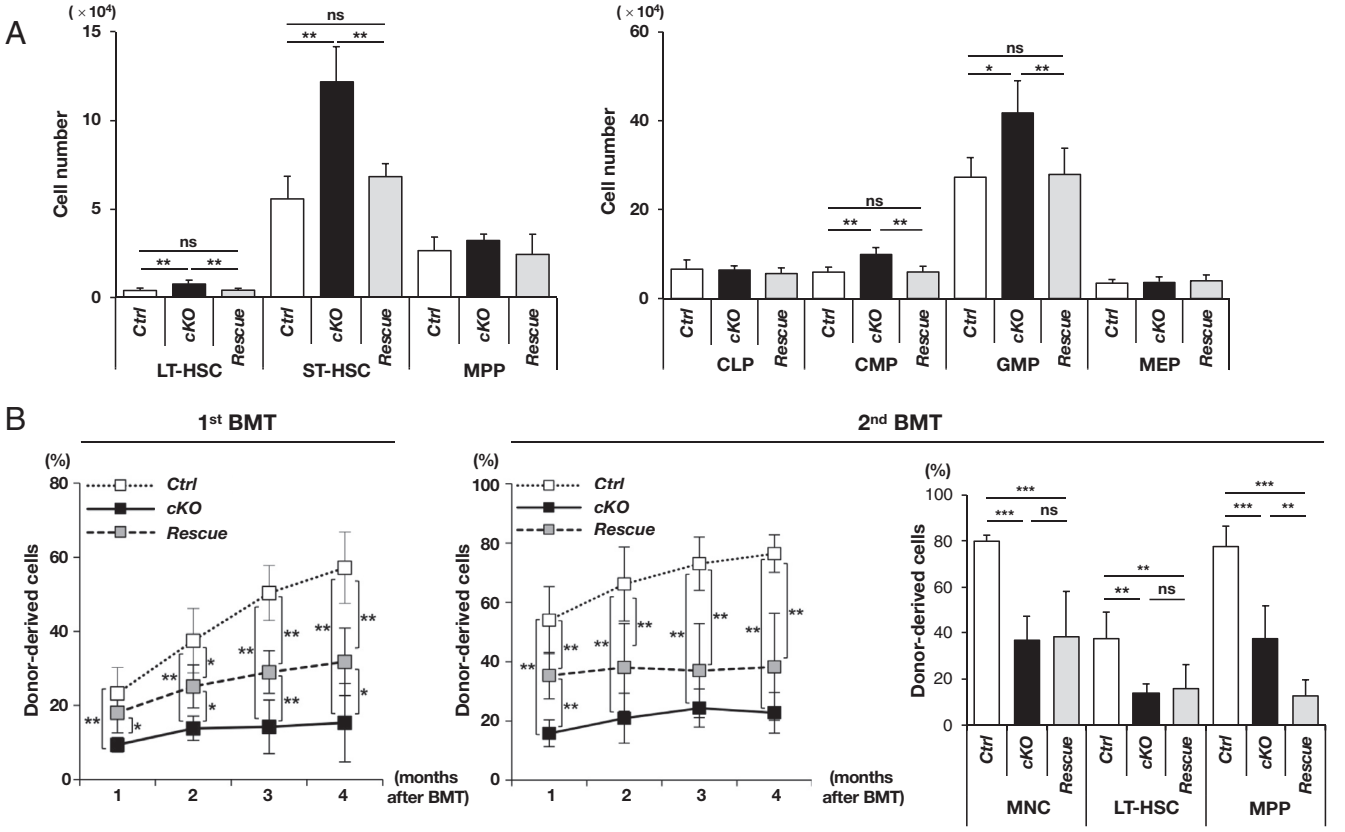

Fig. 4. Restoration of FOXO3a activity normalizes HSPC pool size and partially recovers transplantation capacity of HSCs under *Mbtd1* deficiency. (*A*) Cell numbers in LT-HSC, ST-HSC, and MPP fractions (*Left*) and in CLP, CMP, GMP, and MEP fractions (*Right*) of *CtrlcKO*, and *Rescue* mice (mean ± SD, n = 4 to 6). $^{**}P < 0.01$, $^{*}P < 0.05$, ns: not significant. (*B*) *Left* panel: Donor-derived cells in the PB of the 1st BMT recipients transplanted with *CtrlcKO*, and *Rescue* LT-HSCs at the indicated time points after BMT (mean ± SD, n = 5 to 6). *Right* panel: Donor-derived cells in the PB of the 2nd BMT recipients transplanted with *CtrlcKO*, and *Rescue* BM cells of the 1st transplant recipients at the indicated time points after BMT (mean ± SD, n = 5 to 6). Donor-derived cells in MNC, LT-HSC, and MPP fractions in the BM at the end of BMT (4 mo) are shown. $^{***}P < 0.001$, $^{**}P < 0.01$, $^{*}P < 0.05$, ns: not significant.

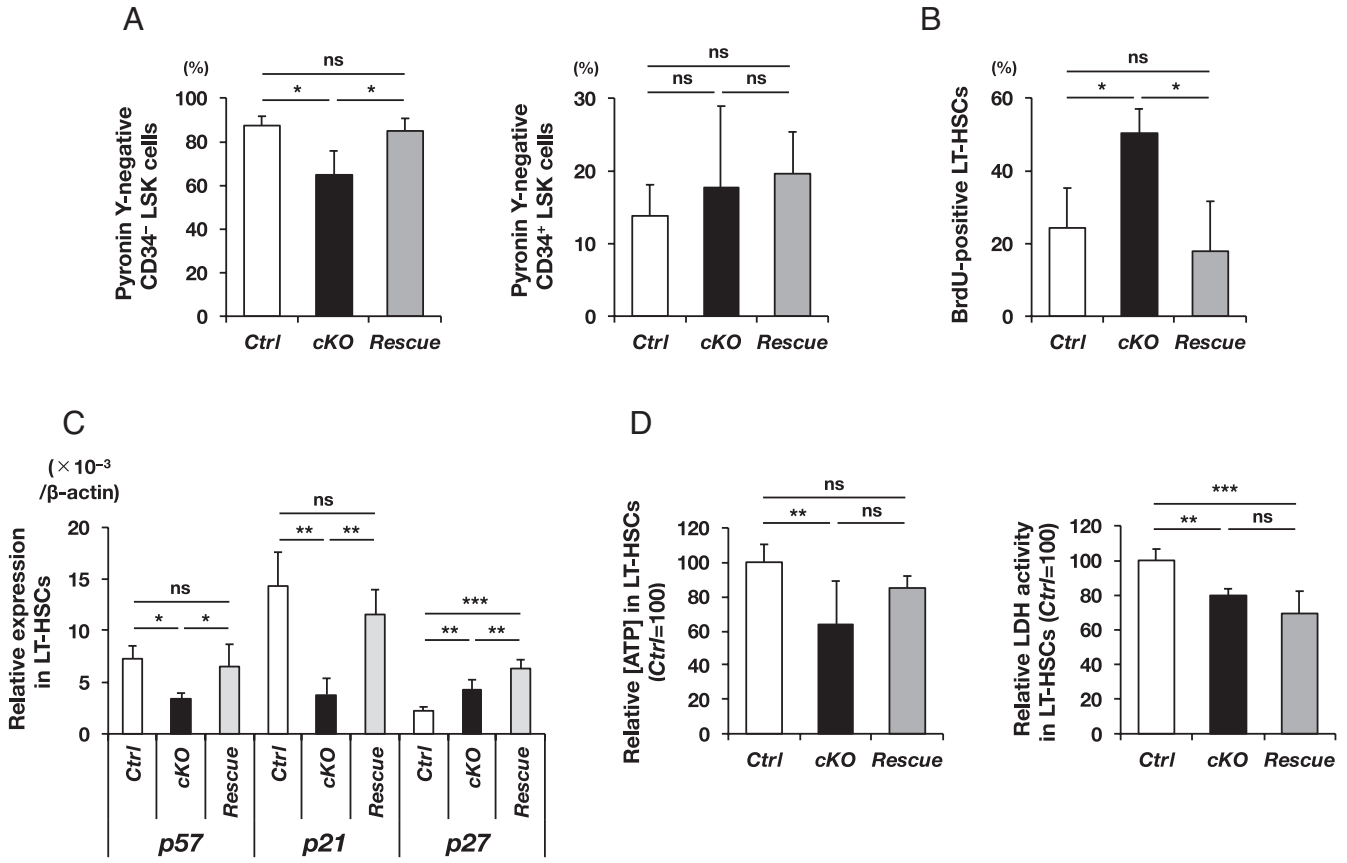

Fig. 5. Cell cycle and metabolic changes in *Mbtd1*-deficient HSCs and recovery of cell cycle defects by restoration of FOXO3a activity. (*A*) Summary of flow cytometric Pyronin Y analysis of $CD34^-$ LSK (*Left*) or $CD34^+$ LSK (*Right*) fractions in *CtrlcKO*, and *Rescu* BM MNCs (mean ± SD, n = 3 to 4). $^*P < 0.05$, ns: not significant. (*B*) Summary of short-term BrdU labeling assay of *CtrlcKO*, and *Rescue* LT-HSCs (mean ± SD, n = 3 to 4). $^*P < 0.05$, ns: not significant. (*C*) qRT-PCR analysis of *p57, p21,* and *p27* in *CtrlcKO*, and *Rescue* LT-HSCs (mean ± SD, n = 4). Each value was normalized to *β-actin*. $^{***}P < 0.001$, $^{**}P < 0.01$, $^*P < 0.05$, ns: not significant. (*D*) Intracellular ATP concentration (*Left*) and LDH activity (*Right*) in *CtrlcKO*, and *Rescue* LT-HSCs (mean ± SD, n = 6). $^{***}P < 0.001$, $^{**}P < 0.01$, ns: not significant.

Identification and Analysis of MBTD1-Interacting Proteins in HSPCs. Given our in vivo studies suggesting that FOXO3a restoration only partially ameliorates HSC properties, MBTD1-binding proteins were investigated to elucidate the MBTD1-regulated pathways. A murine HSPC cell line, EML (29), was used to identify proteins that directly bind to MBTD1. Whole-cell extracts of EML cells were immunoprecipitated using the anti-MBTD1 antibody (9), the immunoprecipitates were digested, and the cleaved fragments were directly analyzed by a direct nanoflow liquid chromatography-tandem mass spectrometry system (Fig. 6*A*). As a result of four repeated assays, the identification of MBTD1 in all experiments and MBTD1-associated TIP60 complex proteins, such as EP400, EPC1, TRPPAP, MRGBP, RUVBL1, and RUVBL2 (17) in more than two independent experiments verified the accuracy of this system (yellow circle in Fig. 6*B* and *SI Appendix*, Table S3). Of note, among repeatedly identified proteins, we found molecules that have been reported to be involved in HSC or other stem cell functions, which included proteins belonging to TIP60 complex (EP400, TRPPAP, RUVBL1, and RUVBL2) (30–33), ribosomal proteins (RPL17, RPL18, and RPS19) (34), heat shock protein (HSPA9) (35), Calmodulin (CaM) (36, 37), and an mRNA regulator (DDX6) (38) (blue circle in Fig. 6*B* and *SI Appendix*, Table S3). It has been shown that sufficient ribosomal function is crucial for suppressing protein synthesis for HSC maintenance (34). In addition, HSPA9 has been suggested to play an essential role in regulating mitochondrial homeostasis in HSPCs (35). These findings indicate that protein synthesis and mitochondrial reactive oxygen species (ROS) production may be altered by MBTD1 deficiency.

Fine-tuning of protein synthesis rate by ribosomal protein is critical for HSC homeostasis (34). Given that MBTD1 interacted with RPL17, RPL18, and RPS19 (Fig. 6*B*), protein synthesis rates of isolated LT-HSCs were analyzed using O-propargyl-puromycin (OP-Puro). Because *Mbtd1*-deficiency changes cell cycle progression in LT-HSCs (Fig. 3 *C* and *D* and *SI Appendix*, Fig. S10), the protein synthesis rate of G0/G1 cells and S/G2/M phases were separately analyzed. OP-Puro uptake in *cKO* LT-HSCs was significantly increased in both phases compared with that observed in *Ctrl* LT-HSCs; however, the OP-Puro uptake observed in *Rescue* LT-HSCs was significantly suppressed and returned to the *Ctrl* level (Fig. 6*C*). In contrast, mitochondrial ROS levels in LT-HSCs were comparable among the three groups (*SI Appendix*, Fig. S14). The physical interaction network of MBTD1-binding proteins (*SI Appendix*, Table S3) predicted by STRING (https://string-db.org/) (39) and clusters of above-mentioned protein groups are summarized in Fig. 6*D*.

Discussion

MBT-containing proteins are a unique class of stem/progenitor cell regulators. L3MBTL2 functions as a critical regulator of pluripotent stem cells and early developmental processes by recruiting a PRC1-related complex in a canonical PRC1/2-independent manner (40). MBT-1/L3MBTL3 was reported to be required for the maturation of myeloid progenitors through *p57* up-regulation (41) and was shown to associate with RNF2/RING1B, an interactor in the polycomb-group (PcG) complex (41). Furthermore,

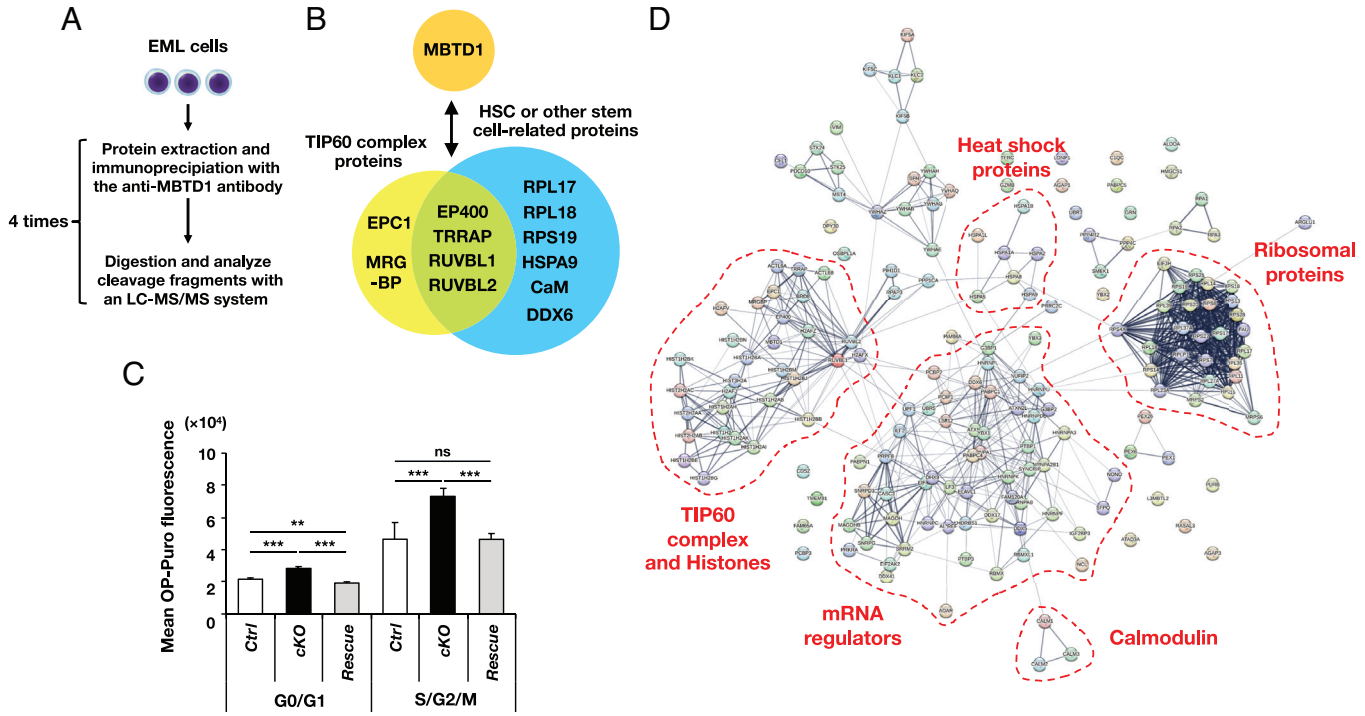

Fig. 6. Identification and analysis of MBTD1-binding proteins. (*A*) Experimental procedure for identification of MBTD1-binding proteins. (*B*) Representative MBTD1-binding proteins identified by mass spectroscopy. TIP60 complex proteins and HSC- or other stem cell-related proteins are shown in yellow and blue circles, respectively. Primary data are shown in *SI Appendix*, Table S3. (*C*) Protein synthesis in LT-HSCs analyzed by OP-Puro. Mean fluorescence intensity of OP-Puro was analyzed using flow cytometry. Cells in G0/G1 or S/G2/M phases were analyzed based on the Hoechst33342 fluorescence (mean ± SD, n = 4 to 7). ***$P < 0.001$, **$P < 0.01$, ns: not significant. (*D*) Interaction network of MBTD1-binding proteins. The physical interaction network of MBTD1-binding proteins (*SI Appendix*, Table S3) predicted by STRING (https://string-db.org) (39) is shown. Clusters of HSC-related proteins are circled by orange dotted lines.

L3MBTL1/H-L(3)MBT is reported to associate with TEL/ETV6, a critical regulator for HSC survival (42).

In this study, we focused on MBTD1, an MBT-containing protein originally identified from an HSC-specific library (8). We previously showed that at E14.5, when the total cell number in the *Mbtd1*$^{-/-}$ FL was severely reduced, *Mbtd1*$^{-/-}$ FL HSCs possessed significantly impaired repopulation ability (9). In addition, by generating and analyzing *Mbtd1*$^{flox/flox}$ mice, we found that acquired *Mbtd1*-deficiency induced HSPC increase and abnormal behaviors of hematopoietic cells under stressful conditions, such as hyperresponsiveness from BM suppression and a defective response after BMT (Figs. 1 and 2). Thus, our findings collectively define MBTD1 as a molecule that governs both fetal and adult HSCs.

To identify the mechanisms that explain the defects in *Mbtd1*-deficient HSCs, we focused on the reduced expression of FOXO3a, which encodes a forkhead family transcription factor and plays a pivotal role in HSC maintenance (26) (Fig. 3*A* and *SI Appendix*, Fig. S8*A*). Given that the response to the 5-FU treatment and repopulation activity of LT-HSC in *cKO* mice closely resemble those in *FoxO3a* KO mice (22, 26), the reduced expression of *FoxO3a* is considered mainly responsible for these abnormal HSC behaviors. Previous studies have shown that FOXO3a exerts its biological effects through regulating the transcription of downstream targets (43), especially Cip/Kip family CDK inhibitors and autophagy-related molecules in HSCs (26, 28). Here, we found that the expression levels of *p57* and *p21* were significantly down-regulated in *cKO* LT-HSCs (Fig. 3*B*). Among these CDKIs, p57 is regarded as a key molecule for LT-HSCs to avoid cell cycle entry and sustain quiescence (44, 45). Our analysis of the cell cycle status of *cKO* LT-HSCs revealed a marked decrease in G0 resting phase ratio and a significant increase in cell proliferation (Fig. 3 *C* and *D* and *SI Appendix*, Fig. S10 *A* and *C*), resulting in an enhanced cell cycle entry. In addition, we demonstrated that MBTD1 directly binds to the promoter region of the *FoxO3a* gene (Fig. 3*E*). Furthermore, restoration of FOXO3a activity in *cKO* mice rescued the cell cycle phenotype and normalized HSPC pool size (Figs. 4*A* and 5 *A*–*C* and *SI Appendix*, Fig. S10 *A* and *C*). Therefore, our results mark MBTD1 as an upstream regulatory molecule of FOXO3a and demonstrate that MBTD1 maintains HSPC pool size by maintaining cell cycle quiescence mainly *via* FOXO3a and downstream CDKIs.

It is noted that there are several discrepancies between the phenotypes of *cKO* and *FoxO3a*-deficient mice. One notable difference is the distinct expression patterns of CDKIs. In LT-HSCs from *cKO* mice, the expression levels of *p57* and *p21* were significantly down-regulated, while *p27* expression was significantly up-regulated (Fig. 3*B*). Conversely, in CD34^{-} LSK cells lacking *FoxO3a*, the expression levels of *p27* and *p57* were significantly down-regulated, while *p21* expression remained unchanged (26). Another discrepancy pertains to the cell cycle status of HSCs. *cKO* LT-HSCs exhibited enhanced cell cycle entry (Fig. 3 *C* and *D*). In contrast, germline loss of *FoxO3a* led to increased HSC cycling, whereas inducible loss of *FoxO3a* had limited impact on HSC cycling (25, 26). The observed changes in cell cycle of LT-HSCs following inducible *Mbtd1* loss, coupled with reduced *FoxO3a* expression, displayed an intermediate phenotype compared with the *FoxO3a* mutants. These findings strongly support the notion that MBTD1 plays a role in regulating the functional integrity of HSCs through mechanisms involving factors beyond FOXO3a. The results from serial BMT experiments further supports this idea, as the chimerism of the *Rescue* group exhibited improvement compared with the *cKO*

group during primary transplantation and in the early stages of secondary transplantation; however, this effect was not sustained in the late phase of secondary transplantation (Fig. 4*B*). In fact, proteomic analysis revealed that MBTD1 interacts with a variety of binding partners (Fig. 6*D*).

The nature of MBTD1 binding to the *FoxO3a* locus remains elusive. MBTD1 was reported to be recruited to genomic sites associated with active transcription as a component of TIP60 chromatin remodeling complex (17, 18). Intriguingly, analysis of the levels of TIP60 recruitment and the deposition of its substrate acetylated H2A.Z (acH2A.Z) identified in mouse FL c-kit$^+$ cells by ChIP-seq (46) revealed strong correlations with P1 and P2 regions and a relatively weak correlation with P3 region of the *FoxO3a* gene (*SI Appendix*, Fig. S15), where MBTD1 was shown to be directly recruited (Fig. 3*E*). These findings raise the possibility that MBTD1 promotes FOXO3a expression, at least in part, as a component of TIP60 complex.

Metabolic regulation including energy production is a critical mechanism that maintains the homeostasis and stress response of HSCs (6). Loss of MBTD1 resulted in decreased glycolytic gene expression, lower ATP levels, and decreased LDH activity in HSCs (Fig. 5*D* and *SI Appendix*, Fig. S13), suggesting a role of MBTD1 in ATP production. Interestingly, restoration of FOXO3a activity rescued cell cycle phenotypes but not metabolic phenotypes in *cKO* HSCs (Figs. 4 and 5). Therefore, we deduced that MBTD1 regulates HSC metabolism *via* a FOXO3a-independent pathway, which may account for the persistent defect in the serial transplantation capacity of *Rescue* HSCs (Fig. 4*B*). FOXO3a-independent regulation of HSCs by MBTD1 may be partially explained by a binding network of MBTD1 (Fig. 6*D*). Among them, TIP60 complex constituents (EP400, EPC1, TRPPAP, MRGBP, RUVBL1, and RUVBL2), ribosomal proteins (RPL17, RPL18, and RPS19), heat shock protein (HSPA9), and Calmodulin (CaM) have been reported to be essential for HSC function (30–37). Interestingly, MBTD1 deficiency-induced abnormal protein synthesis was partly recovered by *FoxO3a^{TM}* (Fig. 6*C*), suggesting a possible contribution of MBTD1-FOXO3a axis to proteostasis in HSCs.

In summary, we demonstrated that MBTD1 plays a pivotal role in adult HSC quiescence by directly binding to the *FoxO3a* gene, possibly as a component of TIP60 complex, and regulating the expression of its downstream CDKIs, especially p57. Our results provide further evidence that the FOXO3a-CDKIs pathway is essential for HSC quiescence as we previously proposed (26, 44) and define MBTD1 as an upstream molecule governing this pathway. In addition, we found that MBTD1 represents a molecule regulating HSC metabolic homeostasis in a FOXO3a-independent manner. Further studies will be required to clarify the mechanisms through which MBTD1 binds to its target genes or proteins, how it exerts its biological function, and how it contributes to the overall regulatory mechanisms of HSC homeostasis.

Materials and Methods

Mice. The detailed procedures for the construction of the targeting vector and generation of *Mbtd1$^{flox/flox}$* mice are described in *SI Appendix*. *Mbtd1$^{flox/flox}$* mice were crossed with *Mx1-Cre$^+$* (*Mx1$^+$*) transgenic mice (21) and *FoxO3a$^{+/TM}$* mutant mice (26) to generate *Mbtd1$^{flox/flox}$/Mx1$^+$* and *Mbtd1$^{flox/flox}$/Mx1$^+$/FoxO3a$^{+/TM}$* mice. pIpC was injected interperitoneally to induce Cre expression as previously described (47). All mice were housed according to the guidelines of the Institute of Laboratory Animal Science, Hiroshima University (permission no. 25-7) and Tokyo Women's Medical University (permission no. AE21-023).

Statistics. Mouse survival curves were constructed using the Kaplan–Meier method and compared by the log-rank test using the GraphPad Prism software. Other statistical analyses were performed using Student's *t* test unless otherwise stated.

A complete and detailed description of the methods is provided in *SI Appendix, Supplemental Materials and Methods*.

Data, Materials, and Software Availability. All study data are included in the article and/or *SI Appendix*.

ACKNOWLEDGMENTS. We thank the members of the Institute of Laboratory Animals, Tokyo Women's Medical University, and Department of Disease Models, Research Institute for Radiation Biology and Medicine, Hiroshima University, for mouse care and technical assistance. We also thank Dr. Junji Takeda and the RIKEN BioResource Center for providing us with KY1.1 ES cells and B6-Tg(CAG-FLPe)36 mice (RBRC01834), respectively. This work was in part supported by Human Frontier Science Program Organization Long-Term Fellowship and AMED-CREST (JP22gm1310006) to H.H., and KAKENHI grants from MEXT/JSPS (20K21621, 21H02957, and 22K19550), a grant from Japan Health Research Promotion Bureau, Japan Agency for Medical Research and Development grants (JP20bm0704042 and JP20gm1210011), a grant from the Takeda Science Foundation, Kaketsuken Grant for Young Researchers, and the MEXT Joint Usage/Research Center Program at the Advanced Medical Research Center, Yokohama City University to K.T.

Author affiliations: [a]Department of Stem Cell Biology, Research Institute, National Center for Global Health and Medicine, Tokyo 162-8655, Japan; [b]Medical Department, 7887 Healthcare Call Center, Yangon 11062, Myanmar; [c]Department of Biochemistry, Kindai University Faculty of Medicine, Sayama-shi, Osaka 589-8511, Japan; [d]Field of Human Disease Models, Major in Advanced Life Sciences and Medicine, Institute of Laboratory Animals, Tokyo Women's Medical University, Shinjuku-ku, Tokyo 162-8666, Japan; [e]Health Care Center and Graduate School of Humanities and Sciences, Institute of Environmental Science for Human Life, Ochanomizu University, Bunkyo-ku, Tokyo 112-8611, Japan; [f]Department of Molecular Oncology, Research Institute of Radiation Biology and Medicine, Hiroshima University, Minami-ku, Hiroshima 734-8553, Japan; [g]Department of Microscopic and Developmental Anatomy, Tokyo Women's Medical University, Tokyo 162-8666, Japan; [h]Department of Stem Cell Biology and Medicine, Graduate School of Medical Science, Kyusyu University, Fukuoka 812-8582, Japan; [i]Department of Human Nutrition, Sugiyama Jogakuen University School of Life Studies, Nagoya 464-8662, Japan; [j]Molecular Profiling Research Center for Drug Discovery, National Institute of Advanced Industrial Science and Technology, Tokyo 135-0064, Japan; and [k]Cancer Science Institute of Singapore, National University of Singapore Center for Translational Medicine, Singapore 117599, Singapore

1. A. Wilson, E. Laurenti, A. Trumpp, Balancing dormant and self-renewing hematopoietic stem cells. *Curr. Opin. Genet. Dev.* **19**, 461–468 (2009).
2. A. Nakamura-Ishizu, H. Takizawa, T. Suda, The analysis, roles and regulation of quiescence in hematopoietic stem cells. *Development* **141**, 4656–4666 (2014).
3. A. de Morree, T. A. Rando, Regulation of adult stem cell quiescence and its functions in the maintenance of tissue integrity. *Nat. Rev. Mol. Cell Biol.* **24**, 334–354 (2023).
4. A. Antoniana Batsivari *et al.*, Dynamic responses of the haematopoietic stem cell niche to diverse stresses. *Nat. Cell Biol.* **22**, 7–17 (2020).
5. O. C. Olson, Y. A. Kang, E. Passegué, Normal hematopoiesis is a balancing act of self-renewal and regeneration. *Cold Spring Harb. Perspect. Med.* **10**, a035519 (2020).
6. A. Nakamura-Ishizu, K. Ito, T. Suda, Hematopoietic stem cell metabolism during development and aging. *Dev. Cell* **54**, 239–255 (2020).
7. D. Karigane *et al.*, p38α activates purine metabolism to initiate hematopoietic stem/progenitor cell cycling in response to stress. *Cell Stem Cell* **19**, 192–204 (2016).
8. R. L. Phillips *et al.*, The genetic program of hematopoietic stem cells. *Science* **288**, 1635–1640 (2000).
9. H. Honda *et al.*, Hemp, an mbt domain-containing protein, plays essential roles in hematopoietic stem cell function and skeletal formation. *Proc. Natl. Acad. Sci. U.S.A.* **108**, 2468–2473 (2011).
10. J. Wismar *et al.*, The Drosophila melanogaster tumor suppressor gene lethal(3)malignant brain tumor encodes a proline-rich protein with a novel zinc finger. *Mech. Dev.* **53**, 141–154 (1995).
11. H. Koga *et al.*, A human homolog of Drosophila lethal(3)malignant brain tumor (l(3)mbt) protein associates with condensed mitotic chromosomes. *Oncogene* **18**, 3799–3809 (1999).
12. J. Berger *et al.*, The human homolog of Sex comb on midleg (SCMH1) maps to chromosome 1p34. *Gene* **237**, 185–191 (1999).
13. E. Montini *et al.*, Identification of SCML2, a second human gene homologous to the Drosophila sex comb on midleg (Scm): A new gene cluster on Xp22. *Genomics* **58**, 65–72 (1999).
14. R. Bonasio, E. Lecona, D. Reinberg, MBT domain proteins in development and disease. *Semin. Cell Dev. Biol.* **21**, 221–230 (2010).
15. K. Meier, A. Brehm, Chromatin regulation: How complex does it get? *Epigenetics* **9**, 1485–1495 (2014).
16. J. Eryilmaz *et al.*, Structural studies of a four-MBT repeat protein MBTD1. *PLoS One* **4**, e7274 (2009).

17. K. Jacquet *et al.*, The TIP60 complex regulates bivalent chromatin recognition by 53BP1 through direct H4K20me binding and H2AK15 acetylation. *Mol. Cell* **62**, 409–421 (2016).
18. H. Zhang *et al.*, Structural basis for EPC1-mediated recruitment of MBTD1 into the NuA4/TIP60 acetyltransferase complex. *Cell Rep.* **30**, 3996–4002.e4 (2020).
19. L. E. Purton, Adult murine hematopoietic stem cells and progenitors: An update on their identities, functions, and assays. *Exp. Hematol.* **115**, 1–14 (2022).
20. J. Seita *et al.*, Gene expression commons: An open platform for absolute gene expression profiling. *PLoS One* **7**, e40321 (2012).
21. R. Kühn, F. Schwenk, M. Aguet, K. Rajewsky, Inducible gene targeting in mice. *Science* **169**, 1427–1429 (1995).
22. K. Miyamoto *et al.*, FoxO3a regulates hematopoietic homeostasis through a negative feedback pathway in conditions of stress or aging. *Blood* **112**, 4485–4493 (2008).
23. Y. Sera *et al.*, UTX maintains the functional integrity of the murine hematopoietic system by globally regulating aging-associated genes. *Blood* **137**, 908–922 (2021).
24. Y. Nakamura *et al.*, Isolation and characterization of endosteal niche cell populations that regulate hematopoietic stem cells. *Blood* **116**, 1422–1432 (2010).
25. Z. Tothova *et al.*, FoxOs are critical mediators of hematopoietic stem cell resistance to physiologic oxidative stress. *Cell* **128**, 325–339 (2007).
26. K. Miyamoto *et al.*, Foxo3a is essential for maintenance of the hematopoietic stem cell pool. *Cell Stem Cell* **7**, 101–112 (2007).
27. S. Yamazaki *et al.*, Cytokine signals modulated via lipid rafts mimic niche signals and induce hibernation in hematopoietic stem cells. *EMBO J.* **25**, 3515–3523 (2006).
28. T. T. Ho *et al.*, Autophagy maintains the metabolism and function of young and old stem cells. *Nature* **543**, 205–210 (2017).
29. S. Tsai, S. Bartelmez, E. Sitnicka, S. Collins, Lymphohematopoietic progenitors immortalized by a retroviral vector harboring a dominant-negative retinoic acid receptor can recapitulate lymphoid, myeloid, and erythroid development. *Genes Dev.* **8**, 2831–2841 (1994).
30. T. Fujii, T. Ueda, S. Nagata, R. Fukunaga, Essential role of p400/mDomino chromatin-remodeling ATPase in bone marrow hematopoiesis and cell-cycle progression. *J. Biol. Chem.* **285**, 30214–30223 (2010).
31. J. I. Loizou *et al.*, Histone acetyltransferase cofactor Trrap is essential for maintaining the hematopoietic stem/progenitor cell pool. *J. Immunol.* **183**, 6422–6431 (2009).
32. O. Bereshchenko *et al.*, Pontin is essential for murine hematopoietic stem cell survival. *Haematologica* **97**, 1291–1294 (2012).
33. S. Hong *et al.*, RuvB-like protein 2 (Ruvbl2) has a role in directing the neuroectodermal differentiation of mouse embryonic stem cells. *Stem Cells Dev.* **25**, 1376–1385 (2016).
34. R. A. J. Signer, J. A. Magee, A. Salic, S. J. Morrison, Haematopoietic stem cells require a highly regulated protein synthesis rate. *Nature* **509**, 49–54 (2014).
35. I. Tai-Nagara, S. Matsuoka, H. Ariga, T. Suda, Mortalin and DJ-1 coordinately regulate hematopoietic stem cell function through the control of oxidative stress. *Blood* **123**, 41–50 (2014).
36. C. M. Kitsos *et al.*, Calmodulin-dependent protein kinase IV regulates hematopoietic stem cell maintenance. *J. Biol. Chem.* **280**, 33101–33108 (2005).
37. L. Racioppi *et al.*, Calcium/calmodulin-dependent kinase kinase 2 regulates hematopoietic stem and progenitor cell regeneration. *Cell Death Dis.* **8**, e3076 (2017).
38. Y. Wang, M. Arribas-Layton, Y. Chen, J. Lykke-Andersen, G. L. Sen, DDX6 orchestrates mammalian progenitor function through the mRNA degradation and translation pathways. *Mol. Cell* **60**, 118–130 (2015).
39. D. Szklarczyk *et al.*, The STRING database in 2023: Protein-protein association networks and functional enrichment analyses for any sequenced genome of interest. *Nucleic Acids Res.* **51**, D638–D646 (2023).
40. J. Qin *et al.*, The polycomb group protein L3mbtl2 assembles an atypical PRC1-family complex that is essential in pluripotent stem cells and early development. *Cell Stem Cell* **11**, 319–332 (2012).
41. S. Arai, T. Miyazaki, Impaired maturation of myeloid progenitors in mice lacking novel Polycomb group protein MBT-1. *EMBO J.* **24**, 1863–1873 (2005).
42. P. Boccuni, D. MacGrogan, J. M. Scandura, S. D. Nimer, The human L(3)MBT polycomb group protein is a transcriptional repressor and interacts physically and functionally with TEL (ETV6). *J. Biol. Chem.* **278**, 15412–15420 (2003).
43. H. Huang, D. J. Tindall, Dynamic FoxO transcription factors. *J. Cell Sci.* **120**, 2479–2487 (2007).
44. A. Matsumoto *et al.*, p57 is required for quiescence and maintenance of adult hematopoietic stem cells. *Cell Stem Cell* **9**, 262–271 (2011).
45. P. Zou *et al.*, p57(Kip2) and p27(Kip1) cooperate to maintain hematopoietic stem cell quiescence through interactions with Hsc70. *Cell Stem Cell* **9**, 247–261 (2011).
46. A. Numata *et al.*, Lysine acetyltransferase Tip60 is required for hematopoietic stem cell maintenance. *Blood* **136**, 1735–1747 (2020).
47. Y. Nakata *et al.*, Acquired expression of CblQ367P in mice induces dysplastic myelopoiesis mimicking chronic myelomonocytic leukemia. *Blood* **129**, 2148–2160 (2017).